REPORT DOCUMENTATION PAGE

Form Approved
OMB NO. 0704-0188

1. AGENCY USE ONLY (Leave Blank)	2. REPORT DATE	3. REPORT TYPE AND DATES COVERED
	2004/11/16	Final report, 2000/04/01 - 2003/09/30

4. TITLE AND SUBTITLE

Gradient-Index (GRIN) Lenses by Slurry-Based Three-Dimensional Printing (S-3DP)

5. FUNDING NUMBERS

DAAD19-00-1-0124

6. AUTHOR(S)

Michael J. Cima

7. PERFORMING ORGANIZATION NAME(S) AND ADDRESS(ES)

Massachusetts Institute of Technology, 77 Massachusetts Avenue, Building 12-011, Cambridge, MA 02139

8. PERFORMING ORGANIZATION REPORT NUMBER

01

9. SPONSORING / MONITORING AGENCY NAME(S) AND ADDRESS(ES)

U. S. Army Research Office
P.O. Box 12211
Research Triangle Park, NC 27709-2211

10. SPONSORING / MONITORING AGENCY REPORT NUMBER

01

41073.1-PH

11. SUPPLEMENTARY NOTES

The views, opinions and/or findings contained in this report are those of the author(s) and should not be construed as an official Department of the Army position, policy or decision, unless so designated by other documentation.

12 a. DISTRIBUTION / AVAILABILITY STATEMENT

Approved for public release; distribution unlimited.

12 b. DISTRIBUTION CODE

13. ABSTRACT (Maximum 200 words)

The BaO-SiO2 material system, which has a 2.4 stronger index changing ability than the Al2O3-SiO2 material system, was developed. Barium acetate was used as the dopant source. The pre-sintering treatment was found to be 900 °C for 18 hours in air to convert barium acetate to barium oxide. The sintering condition was found to be 1725 °C for 10 minutes in vacuum. A barium oxide-doped GRIN lens with radial parabolic index variation was fabricated. Its effective focal length was measured to be 14.63 cm in the x direction and 11.14 cm in the y direction. The barium oxide concentration profiles were measured. The theoretical focal lengths were calculated and compared with the effective focal lengths.

14. SUBJECT TERMS

15. NUMBER OF PAGES

35

16. PRICE CODE

17. SECURITY CLASSIFICATION OR REPORT	18. SECURITY CLASSIFICATION ON THIS PAGE	19. SECURITY CLASSIFICATION OF ABSTRACT	20. LIMITATION OF ABSTRACT
UNCLASSIFIED	UNCLASSIFIED	UNCLASSIFIED	UL

NSN 7540-01-280-5500

Standard Form 298 (Rev.2-89)
Prescribed by ANSI Std. 239-18
298-102

Enclosure 1

Gradient-Index (GRIN) Lenses by Slurry-Based Three-Dimensional Printing (S-3DP™)

SUMMARY

The BaO-SiO_2 material system, which has a 2.4 stronger index changing ability than the Al_2O_3-SiO_2 material system, also was developed. Barium acetate was used as the dopant source. The pre-sintering treatment was found to be 900 °C for 18 hours in air to convert barium acetate to barium oxide. The sintering condition was found to be 1725 °C for 10 minutes in vacuum. A barium oxide-doped GRIN lens with radial parabolic index variation was fabricated. Its effective focal length was measured to be 14.63 cm in the x direction and 11.14 cm in the y direction. The barium oxide concentration profiles were measured. The theoretical focal lengths were calculated and compared with the effective focal lengths

TABLE OF CONTENTS

LIST OF FIGURES

LIST OF TABLES

FINAL REPORT

1. Introduction

1.1 Refractive index changing ability of different oxides in silica

Alumina-doped silica GRIN lenses by S-3DP™ have been successfully fabricated and the details have been submitted previously. The Al_2O_3-SiO_2 material system, however, suffers from the low index change due to the fact that alumina can only slightly change the refractive index of silica [1]. It results in a thicker lens thickness to achieve a shorter focal length and hence increases the total printing time since more slurry layers need to be deposited. Dopants with stronger ability to change the refractive index of silica are required to fully utilize the advantages from using S-3DP™. It is known that titania, although having stronger index change ability, makes silica crystallize easily and causes light scattering. Titania can also be reduced during sintering in vacuum since titanium is a transition metal and can have several oxidation states. The reduction of titania can cause coloration in the sintered samples. It is therefore the search for a new dopant with stronger ability to change refractive index focuses on Groups I-A and II-A on the periodic table. The elements in Group I-A, such as lithium, sodium and potassium, are well known to have fast diffusion in glass [2-7]. The fast diffusion of these elements in glass makes them not a good candidate since the sintering temperature of the un-doped and doped silica powder beds in the study are expected to be higher than 1500 °C and the designed concentration profile can be altered. Group II-A elements generally have lower diffusion rate compared with Group I-A elements and will be considered.

The refractive index of an oxide generally can be related to the polarizability of its metal element. The higher polarizability generally results in a higher refractive index. This trend in Group II-A oxide can be seen in Table 1 [8]. Other factors, such as bonding strength and crystal structure, also affect the refractive index. In general, stiffer/stronger bonds interact less with the

light while softer/weaker bonds interact more. The refractive index, as a result, is larger when the bonding strength is weaker. Table 2 lists the bonding strengths and refractive indices of different oxides [8]. The refractive index of silica is different when its crystal structure is different, as shown in Table 3 [8]. The metal oxides are expected to dissolve into amorphous silica to form transparent samples and only less than 5 mol% of the oxides is expected to be used in this study. It is therefore that the majority of the silica glass network is not altered much, i.e. amorphous. Polarizability and bond strength are hence the dominating factors that determine the refractive index of doped silica. Barium oxide which has high polarizability ($39.7\times10^{-24}\,cm^{-3}$) and weak bonding strength (33 kcal/mol) is the best candidate among Group II-A oxides.

Group II-A oxide	Polarizability of element ($x10^{24}$ cm^3)	Refractive index of oxide
BeO	5.6	1.719
MgO	10.6	1.735
CaO	22.8	1.838
SrO	27.6	1.81
BaO	39.7	1.98

Table 1: Refractive indices of oxides and polarizabilities of elements in Group II-A.

Material	Refractive index of oxide	Single-bond strength (kcal/mole)
SiO_2	1.458	106
Al_2O_3	1.761	108
BeO	1.719	63
MgO	1.735	37
CaO	1.838	32
SrO	1.81	32
BaO	1.98	33

Table 2: Refractive indices and bond strengths of oxides.

SiO_2 polymorth	n	Polarizability of element ($*10^{24}$ cm^3)
Vitreous SiO_2	1.458	5.38
Quartz	1.544	5.38
Tridymite	1.475	5.38
Cristobalite	1.484	5.38

Table 3: Refractive indices of silica polymorphs.

1.2 Phase transformation of Group II-A oxides and silica

It has been discussed in previous section that barium oxide is a good candidate for the dopant of silica in terms of its ability to change the refractive index of silica. The processing compatibilities, such as availability of water-soluble salt, solubility of oxide in silica, and crystallization of alkaline earth-doped silica, are yet to be investigated. Water-soluble salts of Group II-A elements are very common, such as magnesium hydroxide ($Mg(OH)_2$) for magnesium, calcium hydroxide ($Ca(OH)_2$) for calcium, and barium acetate ($Ba(OOCCH_3)_2$) for barium. The solubility of alkaline earth oxides in silica can be seen from the phase diagrams of there alkaline earth oxides and silica. The phase diagrams of the MgO-SiO_2 [9], CaO-SiO_2 [10], SrO-SiO_2 [11], and BaO-SiO_2 [12] material systems are shown in Figures 1, 2, 3, and 4, respectively. Table 4 summaries the eutectic compositions as well as the eutectic temperatures of the alkaline earth oxide-silica material systems. It can be seen that the alkaline earth oxides are very soluble in silica and the solubility is in the range between 46 mol% for the MgO-SiO_2 material system and 25 BaO mol% for the BaO-SiO_2 material system. It is well beyond the expecting dopant concentration (<5 mol%) to be deposited in this study. Figure 5 shows the composite phase diagram of the MgO-SiO_2, CaO-SiO_2, SrO-SiO_2, and BaO-SiO_2 material systems at the temperature between 1600 °C and 2200 °C [13]. It can be clearly seen from Figure 5 that the BaO-SiO_2 material system does not have a two-liquid phase region as the MgO-SiO_2, CaO-SiO_2, and SrO-SiO_2 material systems do. The lack of two-liquid phase region in the BaO-SiO_2 material system makes it the best candidate among the other Group-II-A oxides because BaO and SiO_2 tend not to have phase separation during sintering. The formation of intermediate compounds of BaO and SiO_2, which decreases the transparency of the sample, can be prevented by having appropriate sintering temperature and short sintering time. It is thus, from the discussions in this

section and previous section, that the $BaO\text{-}SiO_2$ material system is the best candidate in terms of index changing ability and sintering possibility. The sintering conditions will be discussed later.

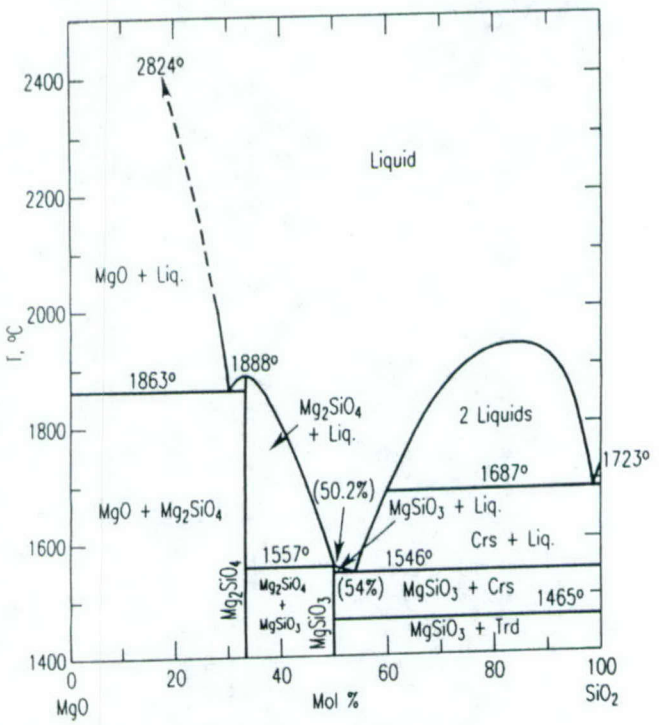

Figure 1: The $MgO\text{-}SiO_2$ phase diagram [9].

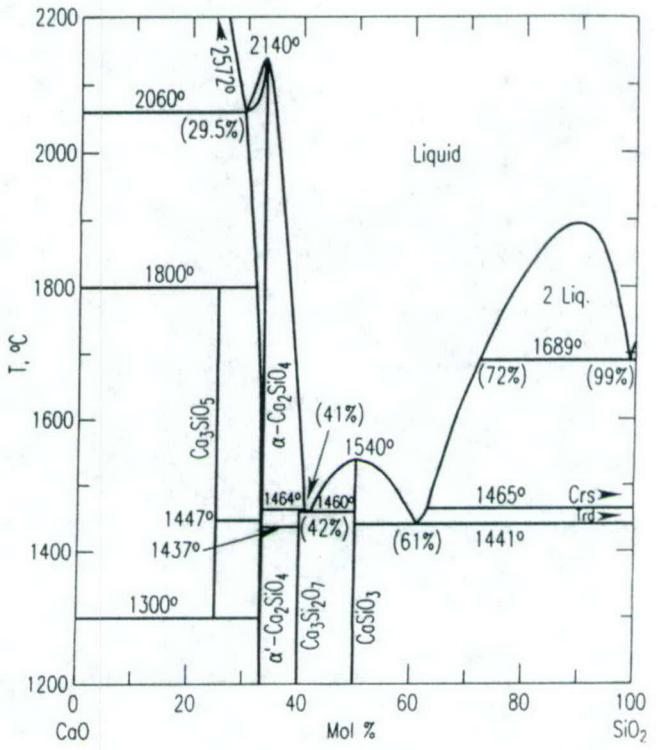

Figure 2: The CaO-SiO_2 phase diagram [10].

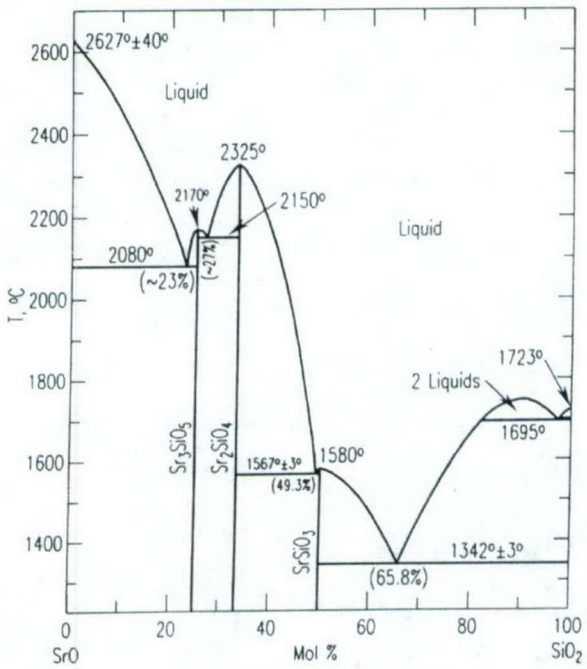

Figure 3: The SrO-SiO_2 phase diagram [11].

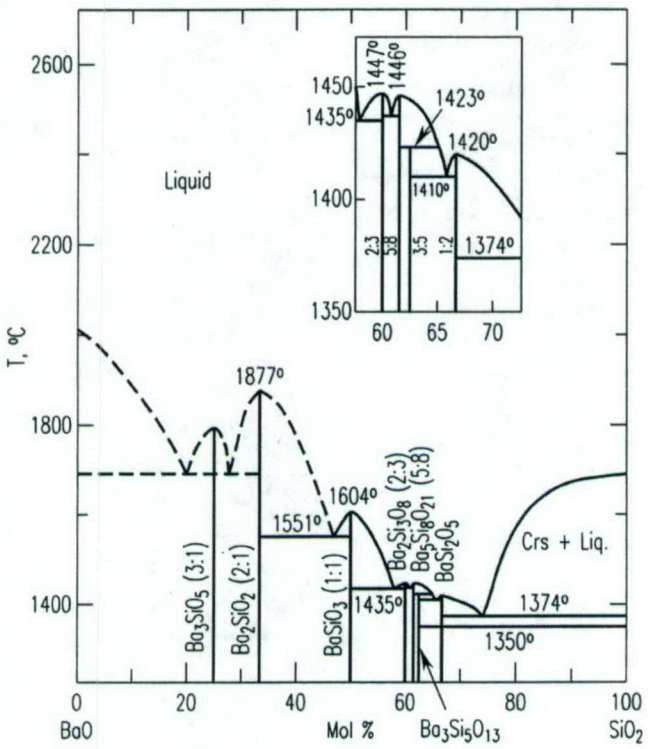

Figure 4: The BaO-SiO_2 phase diagram [12].

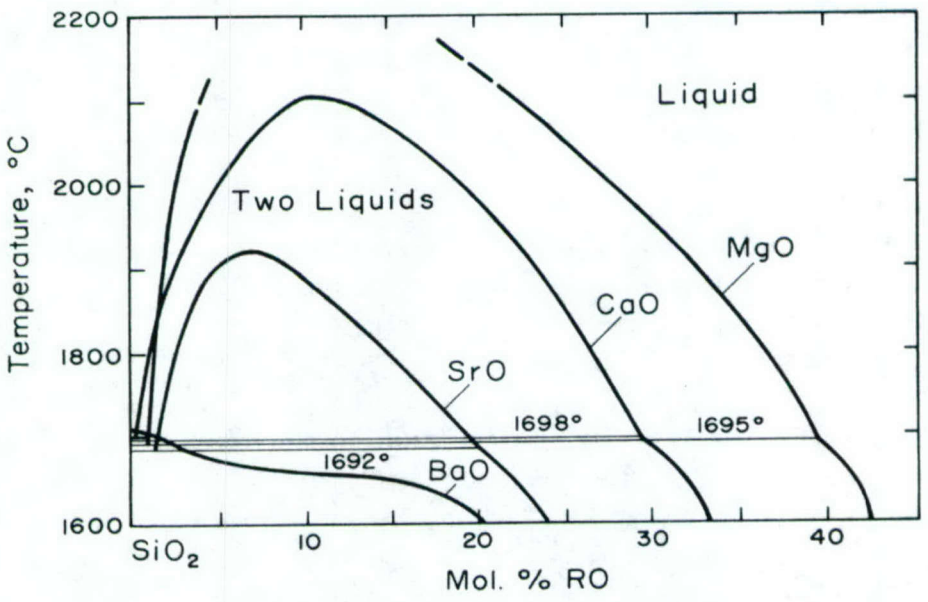

Figure 5: Composite phase diagram of alkaline earth-silica showing immiscibility gap [13].

Material system	Eutectic composition (mol% of alkaline earth oxide)	Eutectic temperature (°C)
$MgO\text{-}SiO_2$	46	1546
$CaO\text{-}SiO_2$	39	1441
$SrO\text{-}SiO_2$	~34	1342
$BaO\text{-}SiO_2$	25	1374

Table 4: Eutectic compositions and temperatures of alkaline earth-silica material systems.

2. Experimental procedures

2.1 Materials

The amorphous silica powder (Silica Ace QS-2, Mitsubishi Chemical Company) used in this research had a median particle size of 1.4 μm and a surface area of 2.666 m^2/g. Barium acetate ($Ba(OOCCH_3)_2$, Alfa Aesar) was used as the dopant source. Radial index variation GRIN lenses were fabricated from a 22.5 vol% slurry. The slurry was ball-milled with glass media (A-285, Potters Industries Inc.) for 20 hours before printing. The chemical composition of the slurry is shown in Table 5. Boric Acid was added to lower the sintering temperature.

Silica Powder (vol%)	Deionized Water (vol%)	Methanol (vol%)	2-Propanol (vol%)	Poly (ethylene glycol) (MW:400)	TMAH* (M)	NH_4OH (M)	H_3BO_3 (wt%)
22.5	38.75	0	38.75	0	0.063	0	1 wt% based on silica

*tetramethylammonium hydroxide

Table 5: The chemical composition of the silica slurry.

2.2 Printing

The TDK 3DP™ machine was used to print barium acetate-doped samples. Barium acetate-doped silica powder beds with radial compositional variation were made with a 3DP™ machine equipped with Drop-on-Demand (DoD) printing nozzles, which allow the dopant solution to be deposited in selective region drop by drop. The DoD printing nozzle has a diameter of 40 μm. An aqueous solution of 18.1 wt% barium acetate was dissolved in water and used as the dopant solution. The drop size of the barium acetate solution was 45 μm. The mass flow rate of the slurry was adjusted so that the thickness of each dried slurry layer was 40 μm. The designed concentration profile is shown in Figure 6. Each printed slurry layer and each printed dopant layer were dried in a microwave oven for 1 minute.

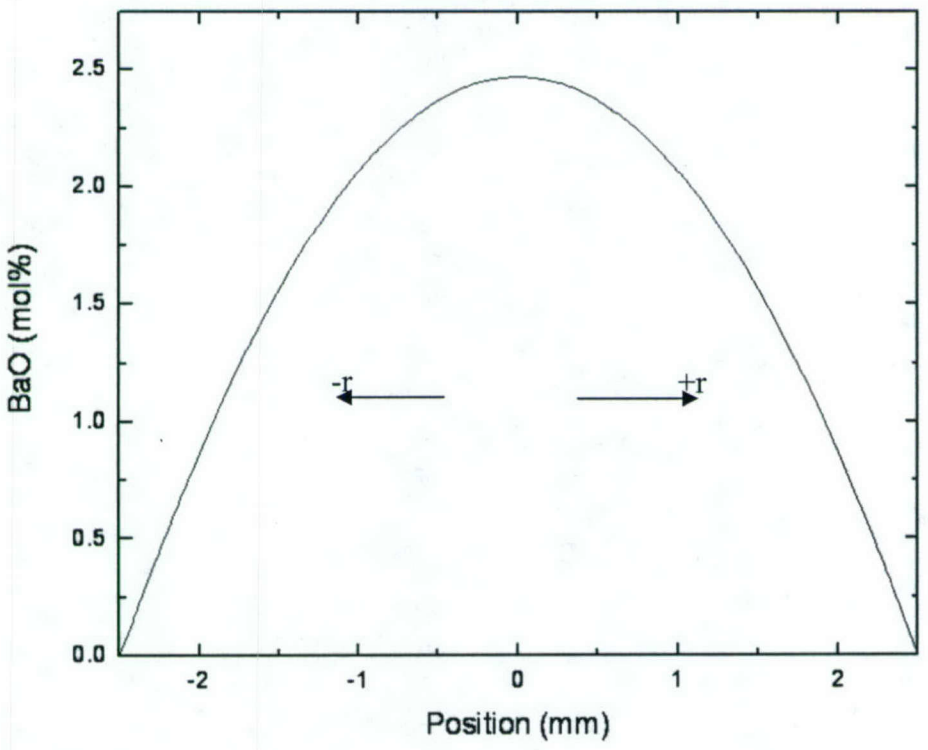

Figure 6: The concentration profile of BaO of the GRIN lens with radial index variation

2.3 *Characterization*

X-ray Diffraction (XRD) was used to detect crystallization of the doped powder bed after heat treatment. The sintered powder beds were polished and observed under an optical microscope (BH-2). Chemical compositions of the doped powder beds were measured by electron probe microanalysis (EPMA, JOEL Superprobe 733). Thermal gravity analysis (TGA, Perkin Elmer)) was used to measure the weight change during different heat treatments.

2.4 *Heat treatment and sintering*

The barium acetate-doped silica powder beds have to be heated to convert barium acetate to barium oxide. Barium acetate powder was heated at different temperatures and times using TGA. XRD was used to determine the phase of residual material after heating. The details of the TGA and XRD results will be shown in the following section. Heat treatment at 900 C for 18 hours in air was used. Several sintering conditions were tested to obtain transparent samples. It was found the sintering condition to be 1725 °C for 10 minutes in the vacuum furnace.

2.5 *Effective focal length measurement*

A simple apparatus, as schematically shown in Figure 7, was used to measure the effective focal length (f_{eff}) of GRIN lens. A GRIN lens was placed on the top of a "MIT" marker with a distance of S. The size of the "MIT" marker was measured as H_1 while the size of the maker's image was measured as H_2 by taking its picture with camera. The equivalent drawing of its optical path diagram is shown in Figure 8, where S_1 is the distance between the object and 1st principle plane, S_2 is the distance between the image and 2nd principle plane, H_1 is the object size, H_2 is the image size, d is the lens thickness, and h is the distance between the 1st and 2nd principle

planes. . Two equations can be obtained from the geometrical relationships in Figure 8, as the followings:

$$\frac{H_2}{S_2 + f_{eff}} = \frac{H_2 - H_1}{S_2} \qquad \text{Equation 1}$$

$$\frac{H_1}{f_{eff} - S_1} = \frac{H_2}{f_{eff}} \qquad \text{Equation 2}$$

The relationship between S_1, S_2, and f_{eff} can be found as the followings:

$$\frac{1}{f_{eff}} = \frac{1}{S_2}\left(\frac{H_2}{H_1} - 1\right) \qquad \text{Equation 3}$$

$$\frac{1}{f_{eff}} = \frac{1}{S_1}\left(1 - \frac{H_1}{H_2}\right) \qquad \text{Equation 4}$$

Equations 3 and 4 can be further deduced to:

$$\frac{1}{f_{eff}} = \frac{1}{S_1} - \frac{1}{S_2} \qquad \text{Equation 5}$$

which is the Gaussian Lens Equation [14] when the image is in the same side of the object.

From the lens designs shown in Figure 6, the focal lengths of these GRIN lenses are expected to be long comparing with the distance between the object and principle plane. It is thus that the thin lens approximation can be applied and the distance between the object and the principle plane (S_1) can be set to approximately equal to the distance between the object and the lens (S). Equation 4, as a result, can be rewritten as:

$$\frac{1}{f_{eff}} = \frac{1}{S}\left(1 - \frac{H_1}{H_2}\right) \qquad \text{Equation 6}$$

The variables in the right-hand side of Equation 6 are measurable from the schematic apparatus shown in Figure 7. The effective focal lengths (f_{eff}) of different GRIN lens designs can then be

calculated from Equation 6. They will be compared with the theoretical focal lengths (f_{th}) in the following sections.

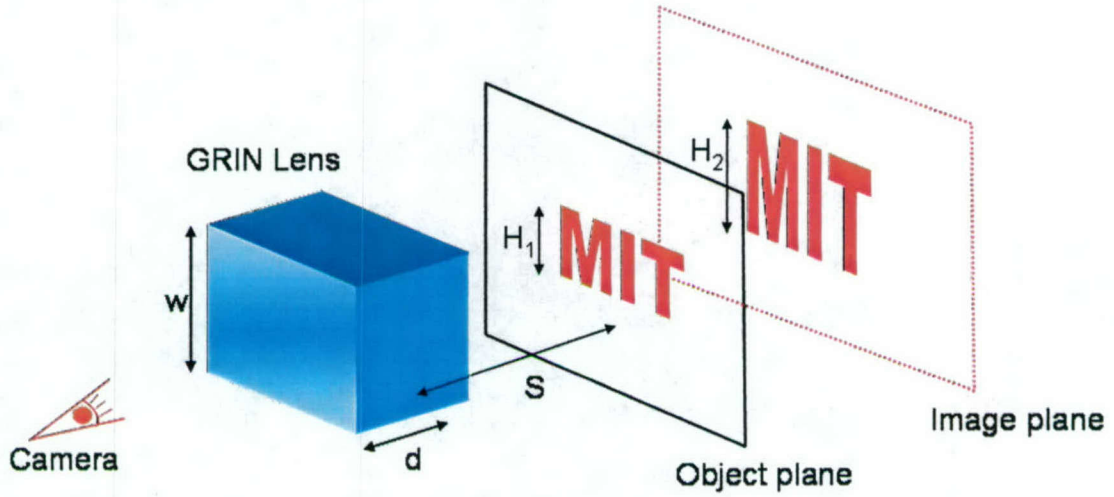

Figure 7: The schematic drawing of the experimental apparatus to measure effective focal length.

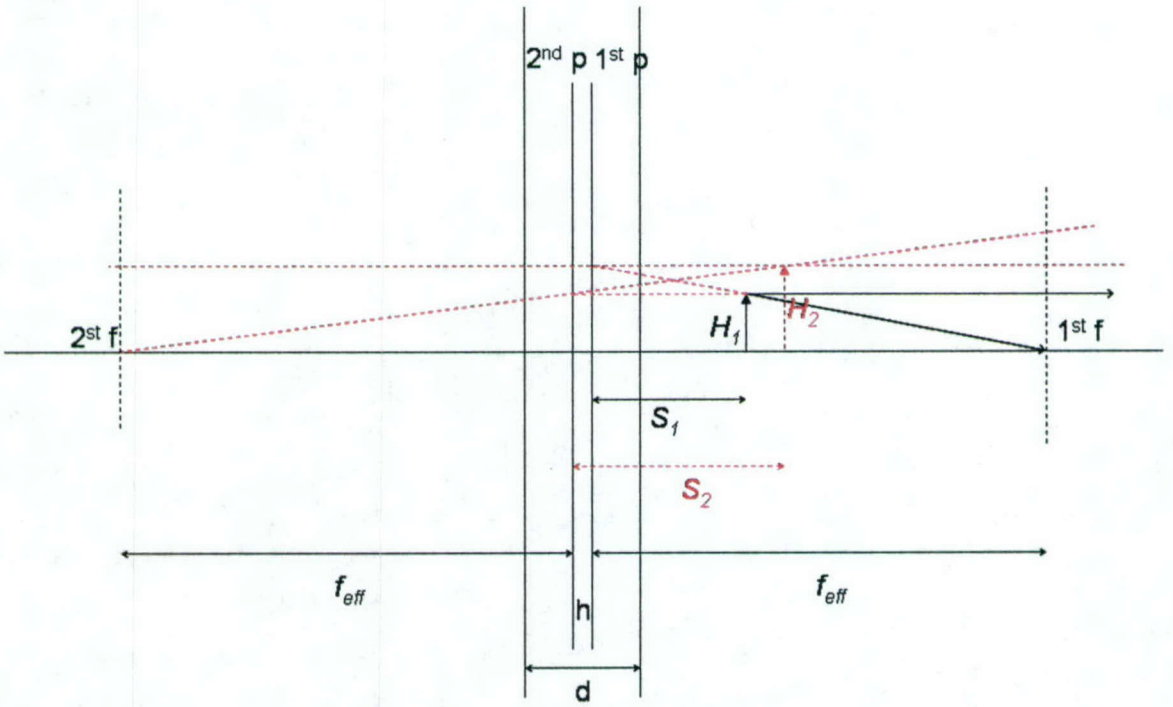

Figure 8: Optical ray-tracing diagram of Figure 7.

3 Results

3.1 Heat treatment of barium acetate

Figure 9 shows the TGA result of barium acetate with a heating rate of 5 °C/min to 1000 °C for 8 hours in air. Barium acetate quickly decomposes to barium carbonate around 500 °C. Further heating of barium carbonate to 1000 °C for 8 hours causes it to gradually decompose to barium oxide. The two-step decomposition reactions are written as the following:

$$Ba(OOCCH_3)_2 + 4O_2 \xrightarrow{\sim 500^\circ C} BaCO_3 + 3CO_2 + 3H_2O \quad \text{(fast)} \quad \text{Equation 7}$$

$$BaCO_3 \xrightarrow{>900^\circ C} BaO + CO_2 \quad \text{(slow)} \quad \text{Equation 8}$$

The residual sample was left at room temperature in air for 12 hours before being measured by XRD and barium carbonate was identified from the XRD result shown in Figure 10. The XRD result is conflict with the TGA result, which shows 100% conversion after heating at 1000 °C for 8 hours. Another TGA experiment was conducted to not measure the weight loss during heating but also the weight change during cooling. The sample was heated 5 °C/min to 1100 °C for 8 hours then cooled 5 °C/min to room temperature. The result is shown in Figure 11. Slight Weight gain during cooling can be seen from Figure 11. It can be explained from Equation 8 that barium carbonate starts to decompose to barium oxide at the temperature higher than 900 °C. Barium oxide can react with carbon dioxide existing in air to form barium carbonate again during cooling. 100% conversion from barium oxide to barium carbonate is possible if the sample is left in air for long enough time. If large amount of barium carbonate exists in the silica powder bed, bubbles would be formed due to the release of carbon dioxide during sintering. It is similar to the bubbles that are formed from the release of water vapor during sintering of aluminum nitrate-doped silica powder bed in the previous report. The heat treatment condition for barium acetate-doped silica powder bed was set to be 900 °C for 18 hours in air to fully convert barium acetate to barium oxide as well as to prevent the silica powder bed from crystallizing at the temperature of

1000 °C or higher. The treated sample was then quickly removed from the furnace and store in a nitrogen glove box. The sample was quickly transferred from the nitrogen glove box to the vacuum furnace right before sintering to minimize the contamination from carbon dioxide.

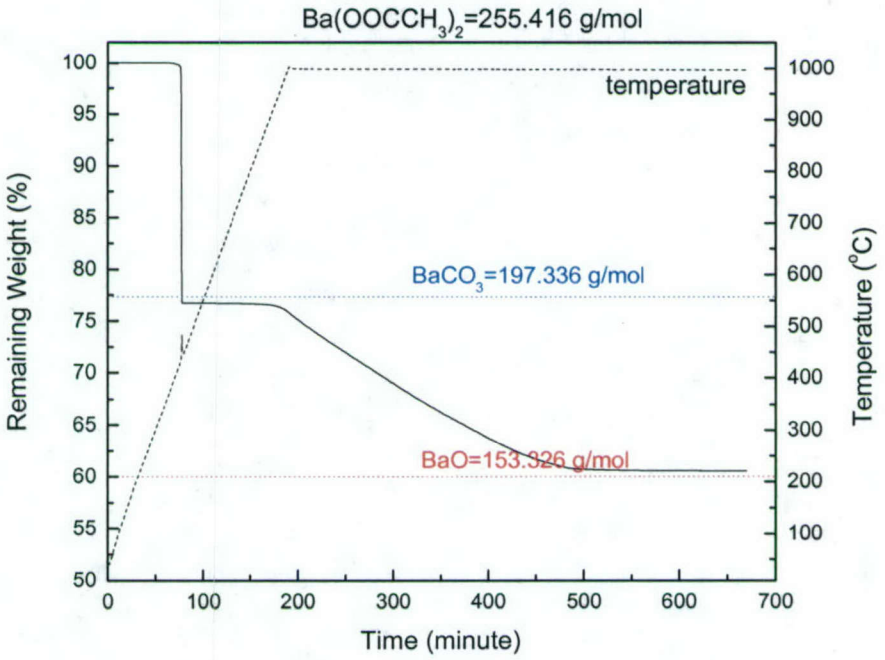

Figure 9: TGA result of barium acetate.

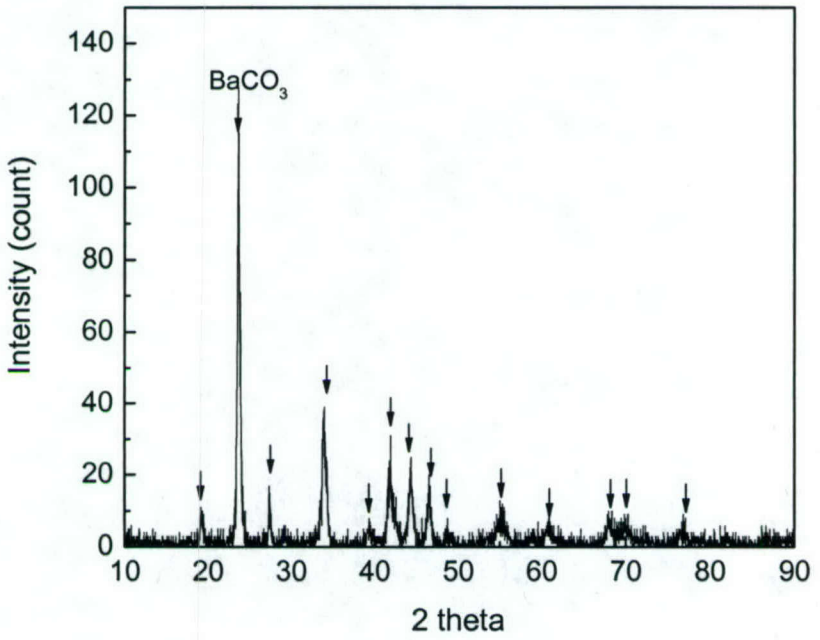

Figure 10: XRD result of the residual sample in Figure 3.9 after being left in air for 12 hours.

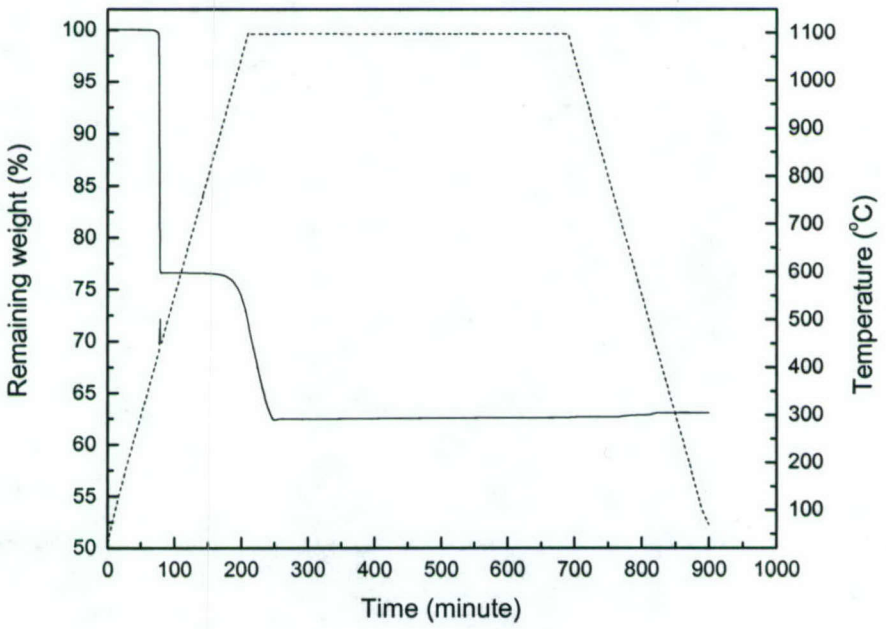

Figure 11: The TGA result of barium acetate with weight gain during cooling.

3.2 Sintering of barium oxide-doped silica powder bed

The sintering study of barium-doped silica powder bed was done based on the result from the Al_2O_3-SiO_2 system. The sintering condition for the Al_2O_3-SiO_2 system is 1650 °C for 30 minutes in vacuum. Silica powder beds printed with one layer of barium acetate line pattern were fabricated to study the sintering condition. The line spacing was 160 μm. These samples were treated at 900 °C for 18 hours to convert barium acetate to barium oxide as described in the previous section. One of the treated samples was then sintered at 1650 °C for 30 minutes in vacuum. It was found that the barium-doped region was crystallized while the un-doped region remains amorphous and transparent, as shown in Figure 12. The crystallized region was identified by XRD as cristobalite, as shown in Figure 13. More sintering conditions were tested on one layer of line pattern or one layer of dot array pattern. The details will be discussed in the following section. The sintering condition was found to be 1725 °C for 10 minutes. A barium oxide-doped silica GRIN lens with a designed concentration profile shown in Figure 6 was sintered. The effective focal length of the sintered barium oxide-doped GRIN lens is measured and the details are given in the next section.

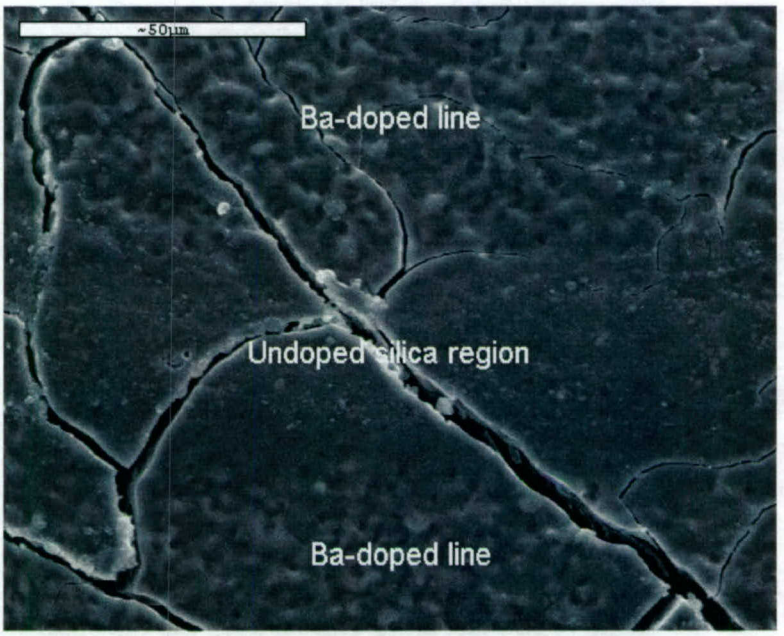

Figure 12: SEM picture of the barium-doped sample with line pattern of 160 μm line spacing sintered at 1650 °C for 30 minutes in vacuum.

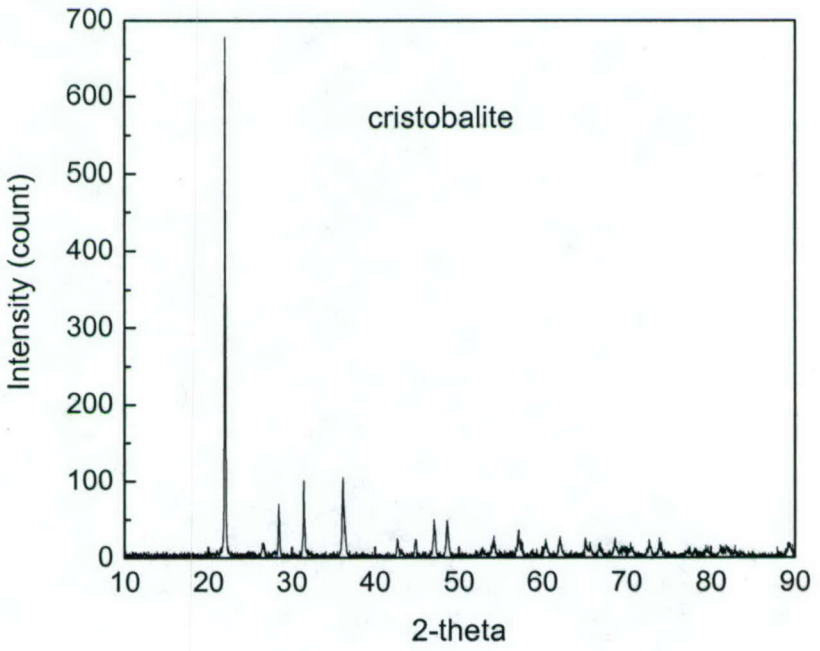

Figure 13: XRD result of the sample in Figure 12

3.3 Effective focal length measurement

The magnifying effect of the sintered barium oxide-doped silica GRIN lens is shown in Figure 14. The MIT marker under the sample is magnified, as expected from the dopant concentration profile previously shown in Figure 6. The object and image sizes as well as the distance between the object and the lens were measured, allowing the effective focal length (f_{eff}) to be determined by Equation 6:

$$\frac{1}{f_{eff}} = \frac{1}{S}\left(1 - \frac{H_1}{H_2}\right) \qquad \text{Equation 6}$$

where H_1 is the object size, H_2 is the image size, and S is the distance between the lens and the object. The effective focal lengths were calculated to be 14.36 cm in the x direction and 11.14 cm in the y direction. The chemical composition profiles in the x direction and the y direction measured by EPMA are shown in Figures 15 and 16. The maximum dopant concentrations in the x direction and the y direction are 2.44 mol% and 2 mol%, respectively.

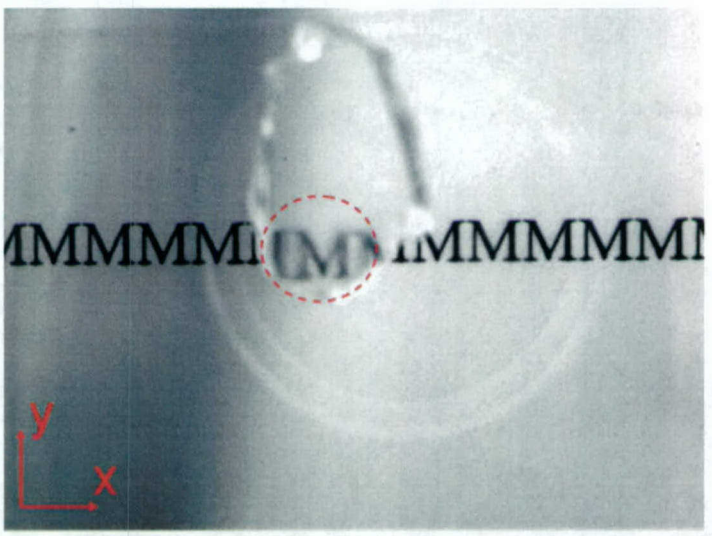

Figure 14: The enlargement with the barium oxide-doped GRIN lenses.

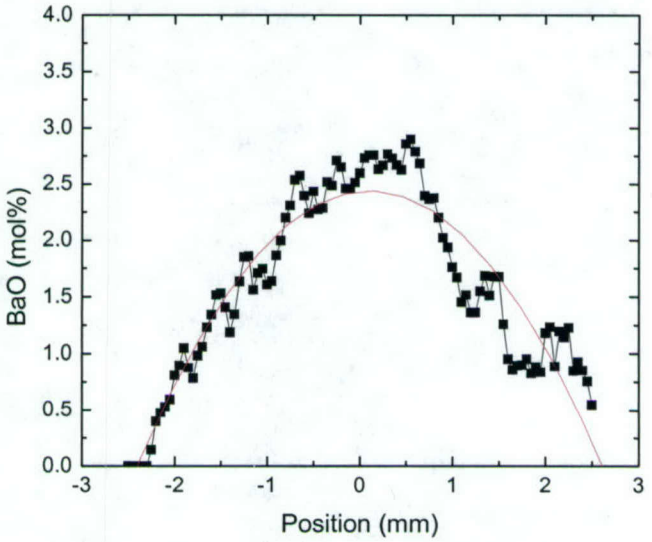

Figure 15: The dopant distribution in the x direction of the barium-doped GRIN lens

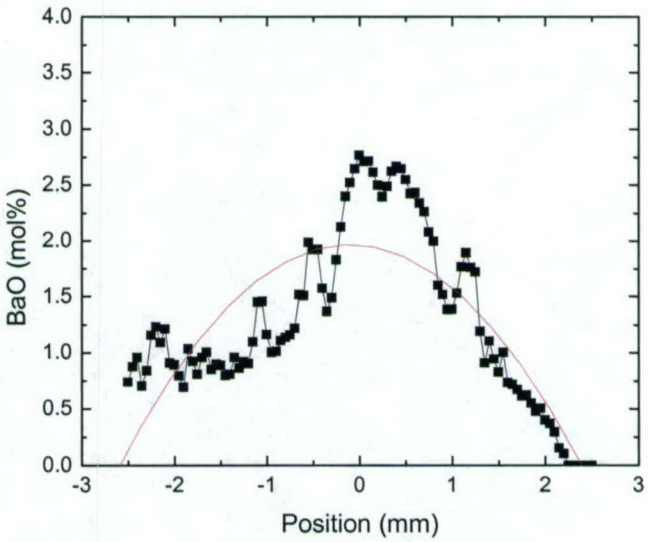

Figure 16: The dopant distribution in the y direction of the barium-doped GRIN lens

4. Discussion

4.1 Sintering of barium oxide-doped silica powder bed

The sintering of the barium oxide-doped sample at 1650 °C for 30 minutes, as described in Section 3.3.2, gives fully densified but crystallized sample. The sintering condition for the Al_2O_3-SiO_2 material system is clearly not suitable for the BaO-SiO_2 material system. The phase diagram of BaO-SiO_2 (Figure 4) shows a liquid-cristobalite region that exists at 1374 °C or higher. It can be understood that cristobalite was detected by XRD in Figure 13. The sintering temperature is high enough to fully sinter the sample but too high that the crystallization rate of critobalite is also fast. The first attempt is to lower the sintering temperature in order to lower the crystallization rate. Sintering at 1500 °C for 30 minutes, which is the sintering condition for undoped silica from Section 2.2.3, is performed on the sample with one layer of line pattern. The sample was fully densified but the line pattern region was still crystallized, as shown in Figure 17. This result indicates that the crystallization rate of cristobalite in the printed region is higher than the sintering rate undoped silica at 1500 °C. It is therefore that lowering sintering temperature to prevent the crystallization does not work in this case. The existing liquid phase in the liquid-cristobalite region does not only help the sintering but also increases the crystallization rate of cristobalite. The second attempt was to increase the sintering temperature close to the melting temperature of vitreous silica, which is about 1725 °C. It was done to melt the cristobalite in the printed region while maintaining the physical shape and chemical composition profile. A series of sintering was done on the samples with one layer of 120 μm-pitch dot array at 1750 °C for different periods of time (0, 1, 2, 5, and 10 minutes). The pictures of the sintered samples are shown in Figures 18 (0 minute), 19 (1 minute), 20 (2 minutes), 21 (5 minutes), and 22 (10 minutes). It can be seen from Figures 18 (0 minute) and 19 (1 minute) that the barium-oxide doped regions are still crystallized. The pictures of the 2-, 5-, and 10-minute samples look like

transparent. Further inspection, however, was done under optical microscope, as shown in Figures 23, 24, and 25. Close observation in Figures 23 and 24 shows cracks around each dot. It indicates that cristobalite is not fully converted to amorphous silica and cracks are generated due the thermal expansion mismatch between cristobalite and amorphous silica during cooling. Cracks are not observed for the sintering times of 10 minutes in Figure 25. It is thus that the sintering of barium oxide-doped GRIN lens with more than one layer of printed pattern is set to be 1725 °C with the sintering time of 10 minutes.

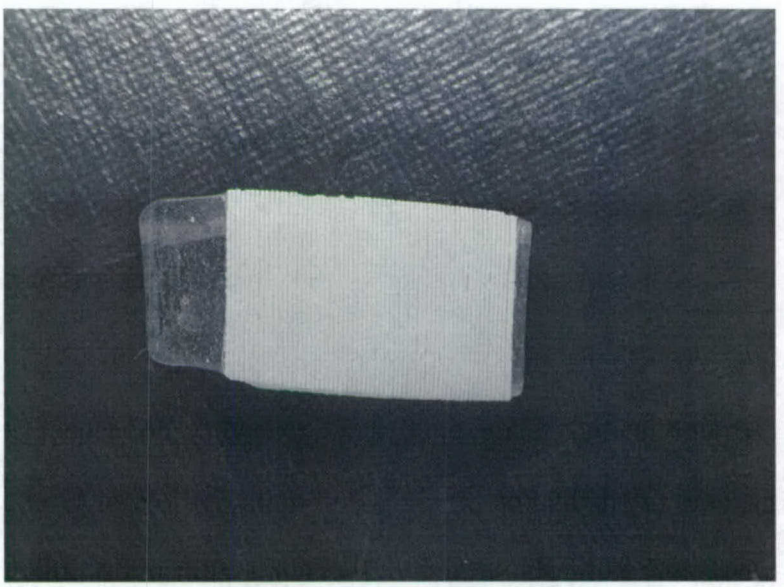

Figure 17: The picture of the barium-oxide doped sample with a 160 μm line pattern sintered at 1500 °C for 30 minutes in vacuum.

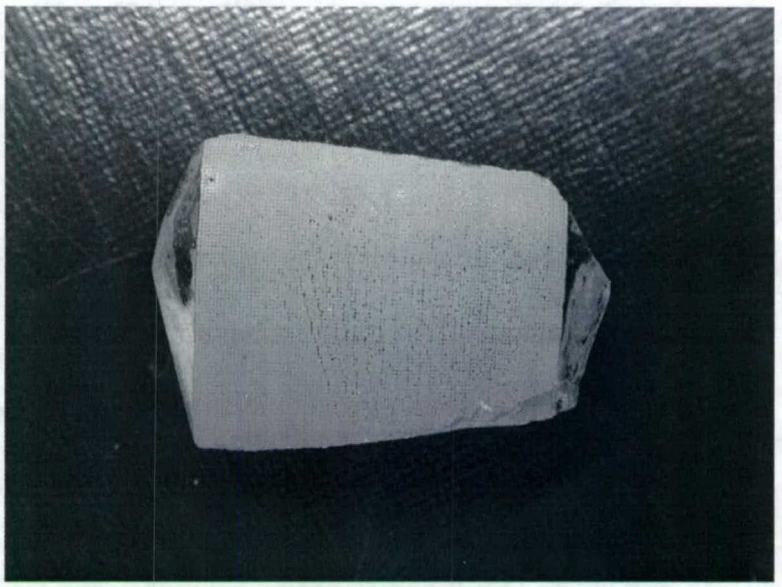

Figure 18: The picture of the barium-oxide doped sample with a 120 μm-pitch dot array sintered at 1725 °C for 0 minutes in vacuum.

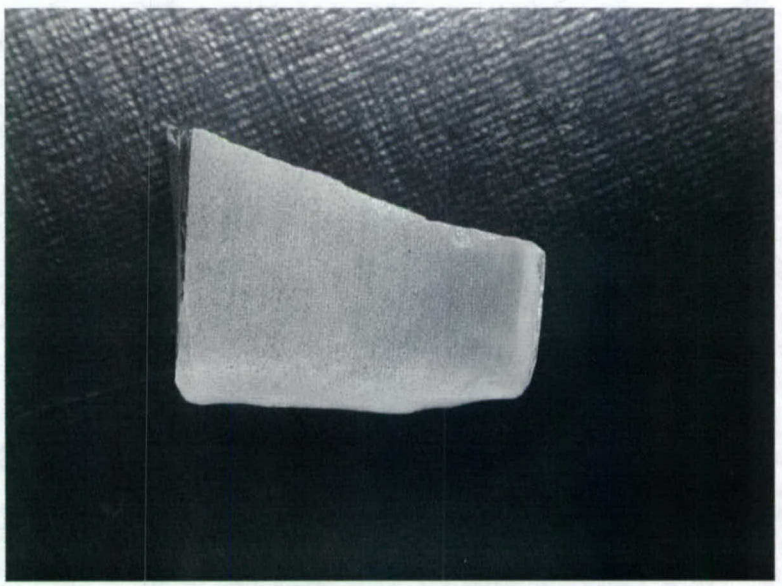

Figure 19: The picture of the barium-oxide doped sample with a 120 μm-pitch dot array sintered at 1725 °C for 1 minute in vacuum.

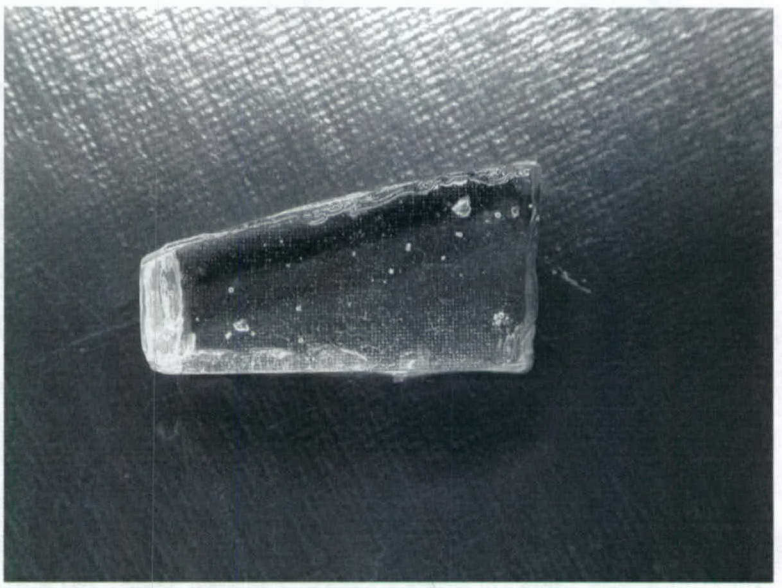

Figure 20: The picture of the barium-oxide doped sample with a 120 μm-pitch dot array sintered at 1725 °C for 2 minutes in vacuum.

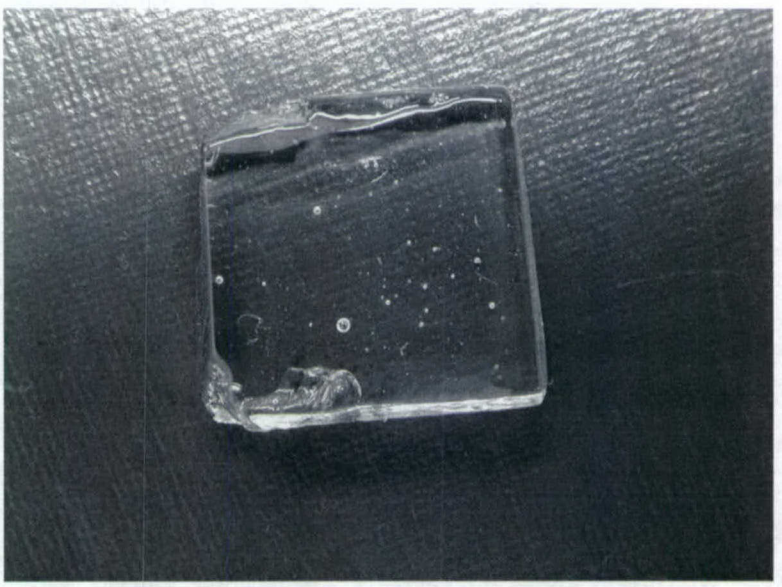

Figure 21: The picture of the barium-oxide doped sample with a 120 μm-pitch dot array sintered at 1725 °C for 5 minutes in vacuum.

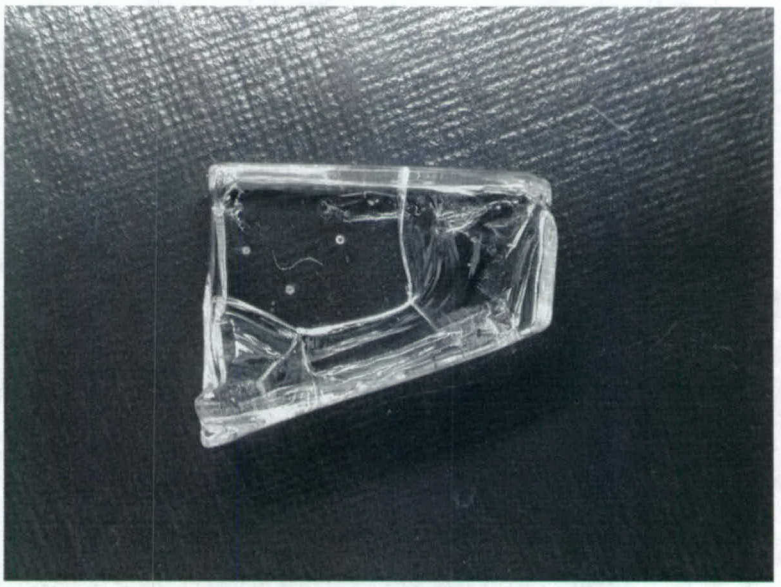

Figure 22: The picture of the barium-oxide doped sample with a 120 μm-pitch dot array sintered at 1725 °C for 10 minutes in vacuum.

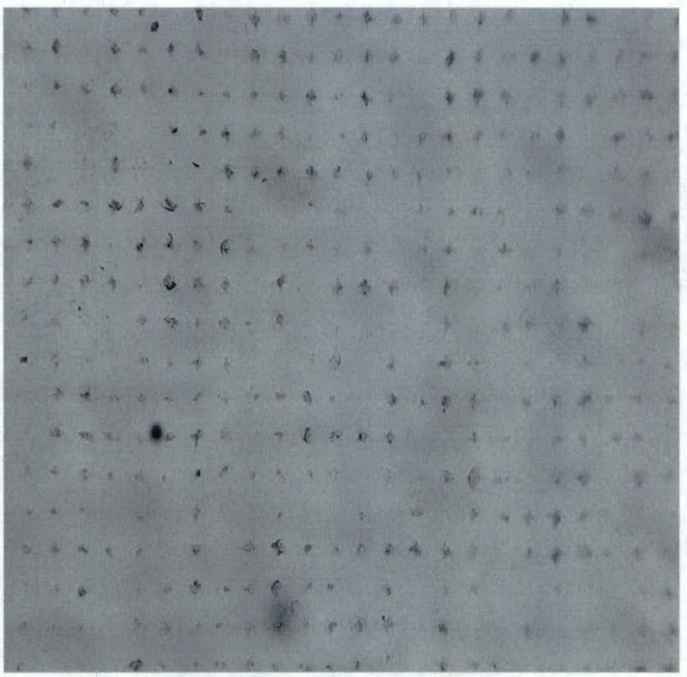

Figure 23: The optical microscopic picture of the barium-oxide doped sample with a 120 μm-pitch dot array sintered at 1725 °C for 2 minutes in vacuum.

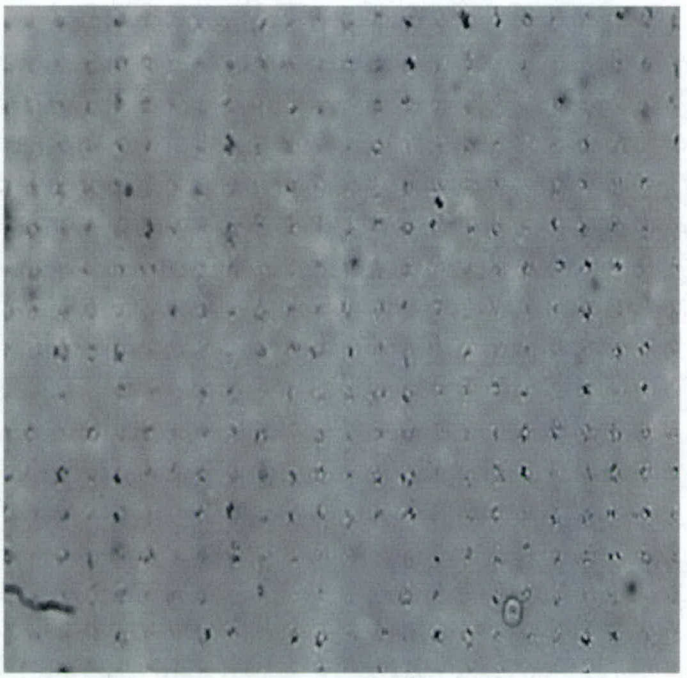

Figure 24: The optical microscopic picture of the barium-oxide doped sample with a 120 μm-pitch dot array sintered at 1725 °C for 5 minutes in vacuum.

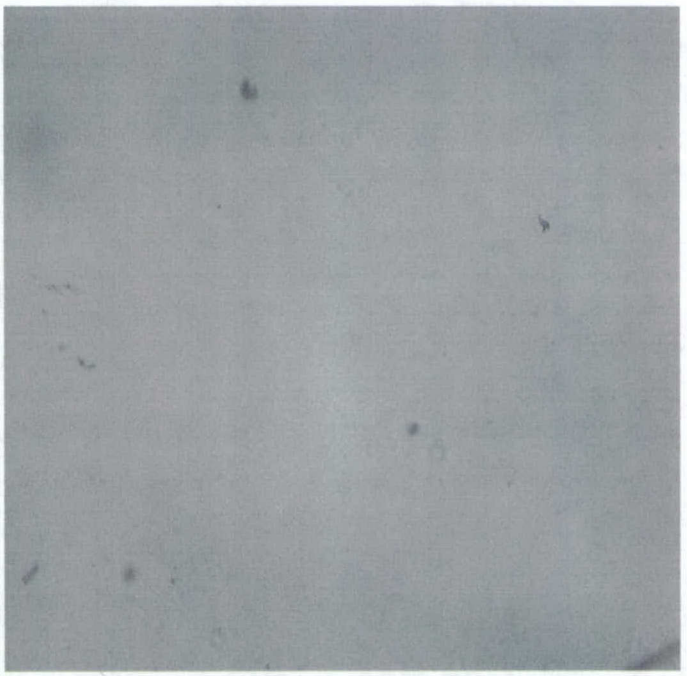

Figure 25: The optical microscopic picture of the barium-oxide doped sample with a 120 μm-pitch dot array sintered at 1725 °C for 10 minutes in vacuum.

4.2 Comparison of effective and theoretical focal lengths

The theoretical focal length (f_{th}) of a GRIN lens with a parabolic refractive index profile is given by the following equation [15]:

$$f_{th} = \frac{1}{\left(\frac{n_{max}^2 - n_{min}^2}{0.25\,w^2}\right)^{1/2} \sin\left(\frac{d}{0.5w}\left(1 - \frac{n_{min}^2}{n_{max}^2}\right)^{1/2}\right)} \qquad \text{Equation 9}$$

where w is the diameter of the GRIN lens, d is the thickness of the GRIN lens, n_{min} is the minimum refractive index, and n_{max} is the maximum refractive index. The diameter and thickness of the GRIN lens are measured to be 0.48 cm and 0.211 cm, respectively. No direct measurement of refractive index has been made in this study. The refractive index, n, of fused silicate containing different amounts of barium oxide, however, can be found in Handbook of Glass Data [16] . The data is plotted together and linearly fitted (R^2>0.99) as shown in Figure 26. It is found that the refractive index of barium oxide-doped silica can be described by the following equation:

$$n=1.4580+0.00467M \qquad \text{Equation 10}$$

where M is the barium oxide concentration in mol%. The barium oxide concentration profiles are fitted with parabolic curves, as previous shown in Figures 15 and 16. The maximum barium oxide concentrations in the x-direction parabolic curve and the y-direction parabolic are found to be 2.44 mol% (Figure 15) and 2.00 mol% (Figure 16), respectively. The maximum refractive indices (n_{max}) in the x direction and the y direction are calculated to be 1.4694 and 1.4673 from Equation 10. The theoretical focal lengths of the sintered powder beds, assuming a parabolic index profile, are then calculated and compared with the effective focal lengths, as shown in Table 6. The theoretical and effective focal lengths both in the x direction and the y direction are close with deviation about 2.5 cm. The small disagreement is resulted from the imperfect parabolic fitting, which can be seen from Figures 15 and 16.

	Effective focal length, f_{eff} (cm)	Theoretical focal length, f_{th} (cm)
x-direction	14.63	12.05
y-direction	11.14	14.68

Table 6: Comparison of effective and theoretical focal lengths of the barium oxide-doped GRIN lens.

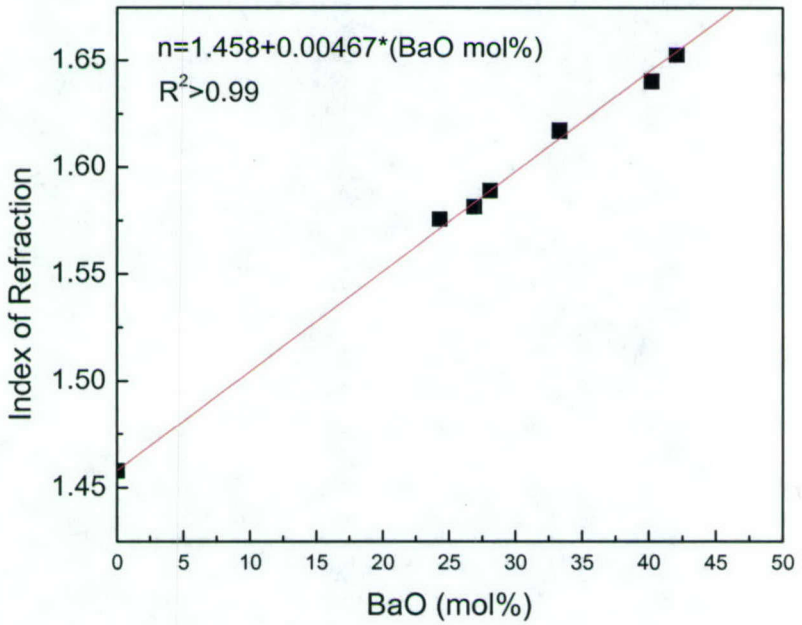

Figure 26: The linear regression result of refractive index of barium oxide-doped silica versus barium oxide concentration.

5. Conclusion

A new material system with higher index changing ability, BaO-SiO_2, has been developed. Barium acetate has been chosen as the water-soluble dopant source. The heat treatment condition to convert barium acetate to barium oxide has been found to be 900 °C for 18 hours in air. It also has been found that the treated sample needs to be put into a moisture-free environment to prevent the absorption of carbon dioxide that converts barium oxide to barium carbonate. Barium

oxide-doped GRIN lenses can be sintered successfully at 1725 °C for 10 minutes in vacuum. The effective focal lengths in x-direction and y-direction have been measured to be 14.63 cm and 11.14 cm, respectively.

6. References

[1] K. Nassau, J. W. Shiever and J. T. Krause, "Preparation and Properties of Fused Silica Containing Alumina," *J. Am. Ceram. Soc.*, **58** [9-10] 461 (1975).

[2] S. I. Sviridov and V. A. Zhabrev, "Diffusion of Singly and Doubly Charged Cations in Sodium Silicate Glasses in the Range 500-800C," *Fiz. Khim. Stekla*, **11** [5] 524-29 (1985).

[3] R. Terai and R. Hayami, "Ionic Diffusion in Glasses," *J. Non-Cryst. Solids*, **18** 217-64 (1975).

[4] V. A. Zhabrev, V. V. Moiseev, S. I. Sviridov and V. G. Chistoserdov, "Diffusion of Divalent Impurity Ions in Vitreous Silica," *The Soviet Journal of Glass Physics and Chemistry*, **2** [4] 326-31 (1976).

[5] V. A. Zhabrev, V. V. Moiseev, S. I. Sviridov and V. G. Chistoserdov, "Sodium Ion Diffusion in Vitreous Silica," *The Soviet Journal of Glass Physics and Chemistry*, **2** [3] 268-72 (1976).

[6] V. A. Zhabrev and S. I. Sviridov, "Ion Diffusion in Oxide Glasses and Melts: I. Bibliography," *The Soviet Journal of Glass Physics and Chemistry*, **29** [2] 140-59 (2003).

[7] G. H. Frischat, "Sodium Diffusion in SiO2 Glass," *J. Am. Ceram. Soc.*, **51** [9] 528--30 (1968).

[8] CRC Handbook of Chemistry and Physics, CRC Press, 2003-2004.

[9] P. Wu, G. Eriksson, A. D. Pelton and M. Blander, "Prediction of the Thermodynamic Properties and Phase Diagrams of Silicate Systems - Evaluation of the Iron(II) Oxide-Magnesia-Silica System," *ISIJ Int.*, **33** [1] 26-35 (1993).

[10] G. Eriksson, P. Wu, M. Blander and A. D. Pelton, "Critical Evaluation and Optimization of the Thermodynamic Properties and Phase Diagrams of the MnO-SiO2 and CaO-SiO2 Systems," *Can. Metall. Q.*, **33** [1] 13-21 (1994).

[11] M. E. Huntelaar, E. H. P. Cordfunke and A. Scheele, "Phase Relations in the Strontium Oxide-Silica-Zirconium Dioxide System I. The System SrO-SiO2," *J. Alloys Compd.*, **191** [1] 87-90 (1993).

[12] M. E. Huntelaar and E. H. P. Cordfunke, "The ternary system barium silicate-strontium silicate-silica (BaSiO3-SrSiO3-SiO2)," *J. Nucl. Mater.*, **201** 250-53 (1993).

[13] E. M. Levin, C. R. Robbins and H. F. McMurdie, Phase Diagrams for Ceramists, American Ceramics Society, Columbus, OH, 1964.

[14] E. Hecht, Optics, Addison-Wesley, 2002.

[15] B. E. A. Saleh and M. C. Teich, Fundamentals of Photonics, John Wiley & Sons Inc., New York, 1991.

[16] O. V. Mazurin, M. V. Streltsina and T. P. Shvaiko-Shvaikovskaya, Handbook of Glass Data, Elsevier, New York, N.Y, 1983.

LIST OF PUBLICATIONS

Peer-Reviewed Journal

Hong-Ren Wang, Michael J. Cima, Brian D. Kernan and Emanuel M. Sachs, "Alumina-Doped Silica Gradient-Index (GRIN) Lenses by Slurry-Based Three-Dimensional Printing (S-3DP^{TM})," *J. Non-Cryst. Solids*, in press, 2004.

Conference Proceedings

Hong-Ren Wang, Michael J. Cima, Brian D. Kernan and Emanuel M. Sachs, "Gradient-Index (Grin) Lenses and Other Optical Elements by Slurry-Based Three Dimensional Printing," American Ceramic Society Annual Meeting (2004), in press.

Hong-Ren Wang, Michael J. Cima, "Alumina-Doped Silica Gradient-Index (GRIN) Lenses by Slurry-Based Three-Dimensional Printing (S-3DP^{TM})," Materials Research Society Symposium Proceedings Series Vol. 758, MRS Fall Meeting (2002).

Hong-Ren Wang, Michael J. Cima, "Three-Dimensional Printing (3DP^{TM}) of Gradient-Index (GRIN) Lenses," Ceramic Transactions Vol. 135, American Ceramic Society Annual Meeting (2002).

Conference Presentations

Hong-Ren Wang, Michael J. Cima, Brian D. Kernan and Emanuel M. Sachs, "Gradient-Index (GRIN) Lenses and Other Optical Elements by Slurry-Based Three Dimensional Printing," invited talk, American Ceramic Society Annual Meeting in Minneapolis, MN. May 2004.

Hong-Ren Wang, Michael J. Cima, Brian D. Kernan and Emanuel M. Sachs, "Barium-doped and Aluminum-doped Silica Gradient-Index (GRIN) Lenses by Slurry-based Three Dimensional Printing (S-3DP^{TM})," Materials Research Society Spring Meeting in San Francisco, CA. April 2004.

Hong-Ren Wang, Michael J. Cima, Brian D. Kernan and Emanuel M. Sachs, "Alumina-Doped Silica Gradient-Index (GRIN) Lenses by Slurry-Based Three-Dimensional Printing (S-3DP^{TM})," The 16th University Conference on Glass Science, Troy, NY. August 2003.

Hong-Ren Wang, Michael J. Cima, Brian D. Kernan and Emanuel M. Sachs, "Alumina-doped Silica Gradient-Index (GRIN) Lenses by Slurry-based Three Dimensional Printing (S-3DP^{TM}) with Drop-on-Demand (DoD) Printing Heads," American Ceramic Society Annual Meeting in Nashville, TN. April 2003.

Hong-Ren Wang, Michael J. Cima, "Alumina-Doped Silica Gradient-Index (GRIN) Lenses by Slurry-Based Three-Dimensional Printing (S-3DP^{TM})," Materials Research Society Fall Meeting in Boston, MA. December 2002.

Hong-Ren Wang, Michael J. Cima, "Three-Dimensional Printing (3DP^{TM}) of Gradient-Index (GRIN) Lenses," American Ceramic Society Annual Meeting in St. Louis, MO. April 2002.